2014 IEEE International Conference on Robotics & Automation (ICRA)
Hong Kong Convention and Exhibition Center
May 31 - June 7, 2014. Hong Kong, China

Modeling and Analysis of an In-Pipe Robotic Leak Detector

Dimitris Chatzigeorgiou, Kamal Youcef-Toumi and Rached Ben-Mansour

***Abstract*— Leakage is the most important factor for unaccounted losses in any pipe network around the world. Most state of the art leak detection systems have limited applicability, lack in reliability and depend on user experience for data extraction. This paper is about a novel system for robotic pipe integrity inspection. Unlike existing systems, detection in based on the presence of a pressure gradient in the neighborhood of a leak. This phenomenon is translated into force measurements via a specially designed and instrumented mechanical embodiment (detector). In this paper an analytic dynamic model of the robotic detector is derived and studied. A prototype is built and the main concepts are validated via experiments.**

I. Introduction

Losses through leaks represent a significant portion of the water supply, hence identification and elimination of leaks is imperative to efficient water resource management [1]. In addition to water losses, there are thousands of miles of natural gas and oil pipelines that are poorly maintained and leaks occur very often [2].

1) Out-of-Pipe Methods: Mays [3] and Hunaidi [4] report on various techniques for leak detection in water pipes. First, water losses can be estimated and identified from water audits. The difference between the amount of water produced by the water company and the total amount of water recorded by usage meters indicates the amount of unaccounted water.

Acoustic leak detection is normally used not only to identify, but also locate leaks [4]. Acoustic devices make contact with valves and/or hydrants or try to listen for leaks on the ground directly above the pipes . Drawbacks of these methods include the necessary experience needed for the operator and the limitation in scalability to the large network range, because the procedure is slow.

More sophisticated techniques use acoustic correlation methods, where two sensors are placed on either side of the leak along a pipeline. The sensors bracket the leak and the time lag between the acoustic signals detected by the two sensors is used to identify and locate the leak [4], [5]. However, a number of difficulties are encountered during the application of the method to plastic pipes and the effectiveness is doubtful [6], [7].

2) In-Pipe Methods: The Smartball is a mobile device that can identify and locate small leaks in water pipelines larger than $10''$ in diameter constructed of any pipe material [8]. The free-swimming device consists of a porous foam ball that envelops a water-tight, aluminum sphere containing the sensitive acoustic instrumentation. In a similar fashion Bond presents a tethered system that pinpoints the location and estimates the magnitude of the leak in large diameter water transmission mains of different construction types [9]. Both Smartball and Sahara are passive and cannot actively maneuver inside complicated pipeline configurations.

In the literature one can find various other in-pipe robots that have been developed for pipe integrity inspection. The vast majority of them are four-wheeled, camera carrying and are intended to be used in gas pipelines, e.g. the EXPLORER [10] and the MRINSPECT [11]. The former one is a long-range, leak-inspection device operating in gas-pipelines and is controlled by an operator in real-time through wireless communication. The operator is constantly looking into a camera to identify leaks.

In this paper we continue our previous research work on the design and development of an in-pipe leak detector [12], [13]. In this work in particular, an analytic dynamic model of the mechanical detector is derived and validated via system identification experiments. Analysis of the model shows that the proposed system can sense leaks at any angle around the circumference of the pipe with only two force sensors, that are carefully positioned on the drum. Finally, the proposed concepts are validated via experiments.

II. Proposed Solution

The concept behind the proposed detection is based on the fact that any leakage in a pipeline alters the pressure and flow field of the working medium. More specifically, there is a fluidic region in the neighborhood of a leak that is characterized by a rapid change in static pressure, dropping from p_{High} inside the pipeline, to p_{Low} in the surrounding medium resting outside. This pressure gradient is apparent in all pressurized pipes in the vicinity of leaks/openings [14]. More importantly, the phenomenon is independent of pipe size and/or material. It also remains relatively insensitive to fluid medium inside the pipes, which makes the detection method widely applicable (gas, oil, water pipes, etc).

However, since a leak can happen at any angle ϕ around the circumference, sensing observability would require a series of pressure sensors installed around the perimeter of the pipe. Nevertheless, directly measuring the pressure at each point in order to calculate the gradient is not effective and should be avoided. To overcome the complexity of such an attempt, we introduce a more efficient concept that is discussed in the next section.

Dimitris Chatzigeorgiou is with the Mechatronics Research Lab, Mechanical Engineering Dept., MIT. Kamal Youcef-Toumi is with Faculty of Mechanical Engineering Dept. and also the director of the Mechatronics Research Lab, MIT. {dchatzis, youcef}@mit.edu

R. Ben-Mansour is with Faculty of Mechanical Engineering Dept., KFUPM. rmansour@kfupm.edu.sa

A. Detection Concept

A schematic of the proposed detection concept is shown in Fig. 1. To capture leaks at any angle ϕ around the circumference a circular membrane is utilized. The membrane is moving close to the pipe walls at all times complying to diameter changes and other defects on the walls, e.g. accumulated scale. The membrane is suspended by a rigid body, called drum (Fig. 1 [a]). The drum is allowed to rotate about its center point G (about any axis) by design. The latter is allowed by a gimbal mechanism, as we demonstrate in detail in the coming section. Finally, the drum is suspended by springs and thus, remains always in the neutral position, when not externally perturbed.

In case of a leak, the membrane is pulled towards it because of the radial drop in pressure (Fig. 1 [b]). Upon touching the wall of the pipe and covering the leak, the pressure difference $\Delta p = p_{High} - p_{Low}$ creates a normal force F on the membrane. We can write that:

$$F = \Delta p A_{Leak} \tag{1}$$

where A_{Leak} stands for the cross-sectional area of the leak, which can be of any shape.

As the system continues to travel along the pipe, a new force, F_z, is generated. This force is a result of friction and contact mechanics between the membrane and the pipe walls. Thus, F_z is related to the normal force, F, by an unknown friction/contact mechanics model, say $F_z = g(F)$. By using Eq. [1] we can see that F_z depends on the pressure difference and the size of the opening, since:

$$F_z = g(\Delta p A_{Leak}) \tag{2}$$

At the next time instant, F_z generates an equivalent force and torque on the drum, M. This torque pushes the drum to rotate about some axis passing through its center point G, while orientation of the axis depends on the angle ϕ of the leak around the circumference (Fig. 1 [c]). The effects of M on the drum can then be sensed by installing force sensors on the detector, as we propose in this paper. Finally, F_z only vanishes when the membrane detaches from the leak and the drum travels back to neutral position, because of the existence of linear springs (Fig. 1 [d]).

In the next section we describe the detailed design of the proposed system that utilizes the concept presented here to effectively identify leaks in pipes. The proposed system can identify a leak by measuring forces on the drum. *Essentially the problem has switched from identifying a radial pressure gradient (at any angle around the circumference of the pipe), to measuring forces on a mechanical detector (gimbal & drum).*

B. Detector Design

A 3D solid model of the proposed detector is presented in Fig. 2. The drum [b] is depicted in red (solid color) and the membrane [a] in dark grey (transparent color). The drum is suspended by a wheeled system. The wheels and the suspension legs [f] are mounted on the front/rear plates

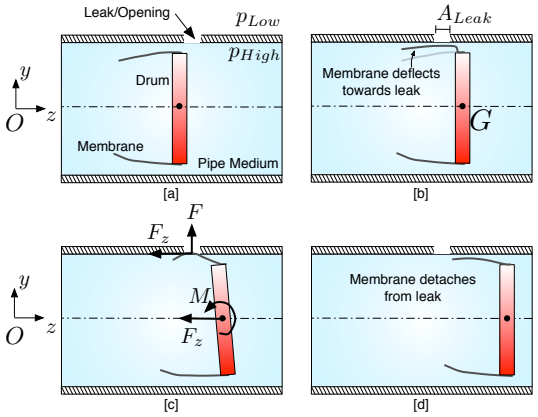

Fig. 1. The detection concept: [a] "Approach Phase": The detector is moving from left to right. [b] "Detection Phase A": The membrane is pulled towards the leak. [c] "Detection Phase B": The membrane touches the walls and covers the leak. [d] "Detaching Phase": Membrane detaches from the leak. Note the inertial reference frame $Oxyz$.

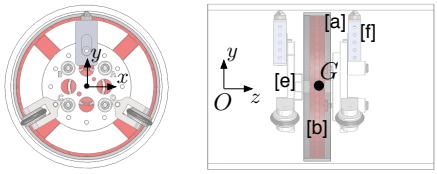

Fig. 2. 3D solid model of the proposed detector. Details: [a] Membrane, [b] Drum, [e] Front Plate and [f] Suspension Legs

[e]. The purpose of the wheels and the suspension legs is to keep the detector always in the middle (collinear with the longitudinal axis) of the pipe during inspection.

A key fact in this design is the gimbal mechanism consisting of two different parts (parts [b] and [c] in Fig. 3). This mechanism allows the drum to pivot about axes x and y at point G independently. We need to mention that the detector we built for the scope of this paper is designed to operate in $100mm$ ID pipes, but the same design can be adopted for pipes with different dimensions by scaling up or down.

In addition, the drum is suspended by four springs [h] as shown in Fig. 3. The purpose of those springs is to drive the drum back to neutral position after the detection phase is over and prepare it for a new detection. The pre-loading of each of those four springs can be independently regulated with help of four setscrews [g]. Finally, the whole system is mounted on a shaft, which essentially represents the chassis of the system [d].

Forces are measured by force sensors. Two such sensors are placed on the drum, behind two of the springs (at distance $r = 17.5mm$ and angles equal to $\alpha = \pi/4$ and $\beta = 3\pi/4$, measured about z axis on the $x-y$ plane, see Fig. 2). As it is shown in the coming sections, such placement of sensors on the drum provides input-observability to the robotic detector, i.e. occurrence of a leak at any angle ϕ (input/disturbance to the detector), results in changes in the measurements.

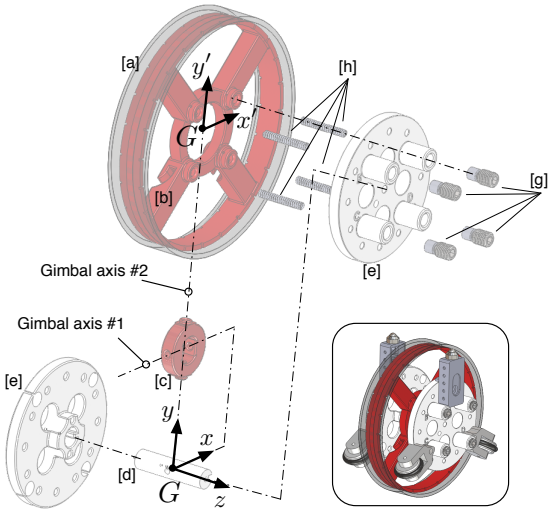

Fig. 3. A 3D assembled view of the detector is shown at the bottom right corner. The exploded view of the proposed design is presented and all key components are laid out. Supporting wheels and suspension legs are omitted for simplicity. Details: [a] Membrane, [b] Drum, [c] Gimbal, [d] Shaft/Chassis, [e] Front/Rear Plates, [g] Spring caps with setscrews, [h] Springs.

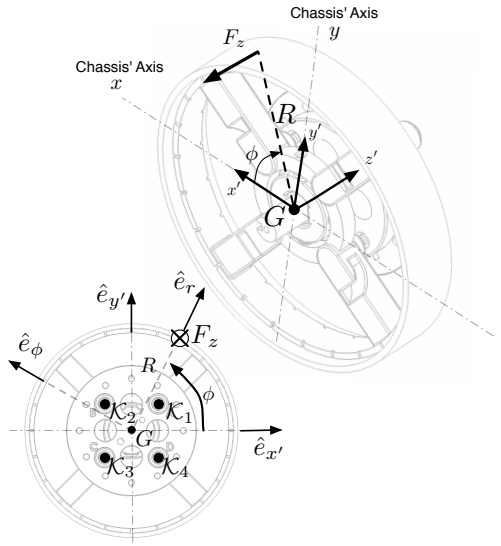

Fig. 4. Force acting on the drum in case of a leak. A 3D view as well as a front view (side) is shown. Note the different frames of reference.

III. Analysis : Dynamic Modeling and Observability

In this section we derive a dynamic model for the proposed robotic detector. The complex nonlinear model is then linearized accordingly to study further. Finally, observability and sensitivity analysis suggest the placement of sensors.

A. Kinematics

Let us assume that the degrees of freedom of the drum & gimbal are $\mathbf{q} = [\theta \ \psi]^T$. Angles θ and ψ measure the rotation of the drum about axis x and y respectively (see Fig. 3 for frames of reference). With this notation the rotation matrix from the body fixed frame (drum) $Gx'y'z'$ to the chassis' frame (chassis of the detector) $Gxyz$ is[1]:

$$\begin{aligned}\mathbf{R}(q) &= \mathbf{R}_y(\psi)\mathbf{R}_x(\theta) \\ &= \begin{bmatrix} c_\psi & 0 & s_\psi \\ 0 & 1 & 0 \\ -s_\psi & 0 & c_\psi \end{bmatrix} \cdot \begin{bmatrix} 1 & 0 & 0 \\ 0 & c_\theta & -s_\theta \\ 0 & s_\theta & c_\theta \end{bmatrix} \\ &= \begin{bmatrix} c_\psi & s_\psi s_\theta & s_\psi c_\theta \\ 0 & c_\theta & -s_\theta \\ -s_\psi & c_\psi s_\theta & c_\psi c_\theta \end{bmatrix} \end{aligned} \tag{3}$$

Let us assume a vector $\mathbf{p}'_\mathcal{K}$ denoting the point $\mathcal{K}$ on the drum with respect to the body fixed frame (drum). If κ is the enclosed angle and $r_\mathcal{K}$ the length of the vector (distance $\overline{\mathcal{K}G}$) we can write:

$$\mathbf{p}'_\mathcal{K} = \begin{bmatrix} x'_\mathcal{K} \\ y'_\mathcal{K} \\ z'_\mathcal{K} \end{bmatrix} = r_\mathcal{K} \begin{bmatrix} c_\kappa \\ s_\kappa \\ 0 \end{bmatrix} \tag{4}$$

[1] c_j stands for $cos(j)$ and s_j stands for $sin(j)$ correspondingly. Similar notation is used throughout this paper for simplicity.

We can write that $\mathbf{p}_\mathcal{K} = \mathbf{R}(q)\mathbf{p}'_\mathcal{K}$ for the transformation of the vector to the chassis' frame. This transformation (using Eq. [3, 4]) gives:

$$\mathbf{p}_\mathcal{K} = \begin{bmatrix} x_\mathcal{K} \\ y_\mathcal{K} \\ z_\mathcal{K} \end{bmatrix} = r_\mathcal{K} \begin{bmatrix} c_\psi c_\kappa + s_\psi s_\theta s_\kappa \\ c_\theta s_\kappa \\ c_\psi s_\theta s_\kappa - s_\psi c_\kappa \end{bmatrix} \tag{5}$$

Taking derivatives with respect to time:

$$\dot{\mathbf{p}}_\mathcal{K} = \begin{bmatrix} \dot{x}_\mathcal{K} \\ \dot{y}_\mathcal{K} \\ \dot{z}_\mathcal{K} \end{bmatrix} = r_\mathcal{K} \begin{bmatrix} -s_\psi c_\kappa \dot{\psi} + c_\psi s_\theta s_\kappa \dot{\psi} + s_\psi c_\theta s_\kappa \dot{\theta} \\ -s_\theta s_\kappa \dot{\theta} \\ -s_\psi s_\theta s_\kappa \dot{\psi} + c_\psi c_\theta s_\kappa \dot{\theta} - c_\psi c_\kappa \dot{\psi} \end{bmatrix} \tag{6}$$

Now that we have established the basic foundation for the next sections, we can proceed with the derivation of the equations of motion for the detector.

B. Dynamic Modeling - Equations of Motion

1) Nonlinear Governing Equations: We discussed earlier that a force $\mathbf{F_z} = -F_z\hat{\mathbf{e}}_\mathbf{z}$ is generated at leak positions[2]. This force is then generating a torque about point G, the center of the gimbal mechanism, which is equal to (Fig. 4):

$$\begin{aligned}\mathbf{M} &= F_z R \hat{\mathbf{e}}_\phi \\ &= \underbrace{-F_z R s_\phi}_{M_x} \hat{\mathbf{e}}_\mathbf{x} + \underbrace{F_z R c_\phi}_{M_y} \hat{\mathbf{e}}_\mathbf{y} \end{aligned} \tag{7}$$

In the previous notation R is the radial distance from the point of the membrane/drum that the force F_z is applied, to the center of rotation G (Fig. 4). This torque (Eq. [7]) represents the input/disturbance of the dynamic model that is discussed in this section. Note that $\hat{\mathbf{e}}_\phi$ is the unit vector along the axis of rotation of the drum, while $\hat{\mathbf{e}}_\mathbf{r}$ is normal to $\hat{\mathbf{e}}_\phi$ and in the radial direction.

[2] we use $\hat{\mathbf{e}}_\mathbf{z}$ to represent the unit vector along axis z and similar notation is followed throughout the paper.

Let us start by defining the state vector $\mathbf{x} = [\theta\ \dot{\theta}\ \psi\ \dot{\psi}]^T$. Assuming there is a spring of stiffness $k_{\mathcal{K}}$ at point $\mathcal{K}$, we can calculate the torque it produces about x and y axes respectively:

$$\begin{aligned} {}^{\mathcal{K}}M_{k,x}(\mathbf{x}) &= k_{\mathcal{K}} z_{\mathcal{K}} y_{\mathcal{K}} \\ &= k_{\mathcal{K}} r_{\mathcal{K}}^2 (c_\psi s_\theta s_\kappa - s_\psi c_\kappa) c_\theta s_\kappa \end{aligned} \tag{8}$$

$$\begin{aligned} {}^{\mathcal{K}}M_{k,y}(\mathbf{x}) &= -k_{\mathcal{K}} z_{\mathcal{K}} x_{\mathcal{K}} \\ &= -k_{\mathcal{K}} r_{\mathcal{K}}^2 (c_\psi s_\theta s_\kappa - s_\psi c_\kappa)(c_\psi c_\kappa + s_\psi s_\theta s_\kappa) \end{aligned} \tag{9}$$

In the previous derivation we used Eq. [5] to evaluate the quantities under discussion. We also assumed for simplicity that the spring torques are equal to zero when the drum rests at neutral position ($\theta = \psi = 0$).

We also assume that there is a linear dashpot of strength $b_{\mathcal{K}}$ at point $\mathcal{K}$ (same point and parallel to the spring element we modeled earlier). We now get the resulting torques about x and y axes that are equal to:

$$\begin{aligned} {}^{\mathcal{K}}M_{b,x}(\mathbf{x}) &= b_{\mathcal{K}} \dot{z}_{\mathcal{K}} y_{\mathcal{K}} \\ &= b_{\mathcal{K}} r_{\mathcal{K}}^2 (c_\psi c_\theta s_\kappa \dot{\theta} - s_\psi s_\theta s_\kappa \dot{\psi} - c_\psi c_\kappa \dot{\psi}) c_\theta s_\kappa \end{aligned} \tag{10}$$

$$\begin{aligned} {}^{\mathcal{K}}M_{b,y}(\mathbf{x}) &= -b_{\mathcal{K}} \dot{z}_{\mathcal{K}} x_{\mathcal{K}} \\ &= -b_{\mathcal{K}} r_{\mathcal{K}}^2 (c_\psi c_\theta s_\kappa \dot{\theta} - s_\psi s_\theta s_\kappa \dot{\psi} - c_\psi c_\kappa \dot{\psi})(c_\psi c_\kappa + s_\psi s_\theta s_\kappa) \end{aligned} \tag{11}$$

In the previous derivation we used Eq. [6] to evaluate the quantities under discussion. The idea of adding linear dashpots to the model is to compensate for the viscous losses observed in the prototyped robotic detector, as shown later in the paper.

We can now extend this framework to come up with the complete nonlinear equations of motion of a drum, that is able to rotate about two axes (2 degrees of freedom) connected to $n = 4$ springs and dashpots at different points ($\mathcal{K}_i$). The governing equations of such a mechanical system that is subject to a leak force F_z (disturbance) as described by Eq. [7] can be given by:

$$\begin{cases} I_{xx}\ddot{\theta} + \sum_{i=1}^{4} \{ {}^{\mathcal{K}_i}M_{b,x}(\mathbf{x}) + {}^{\mathcal{K}_i}M_{k,x}(\mathbf{x}) \} = M_x = -F_z R s_\phi \\ I_{yy}\ddot{\psi} + \sum_{i=1}^{4} \{ {}^{\mathcal{K}_i}M_{b,y}(\mathbf{x}) + {}^{\mathcal{K}_i}M_{k,y}(\mathbf{x}) \} = M_y = F_z R c_\phi \end{cases} \tag{12}$$

I_{xx} and I_{yy} are the moments of inertia of the system about axes x and y respectively. To derive those equations of motion, Eq. [8-11, 7] are used. For the rest of this analysis let us assume that all springs are of identical stiffness k and all linear dashpots have the same strength b for simplicity.

We claim in this paper, that by placing two force sensors at points $\mathcal{A}$ and $\mathcal{B}$ (equal distance r from G, enclosed angles α and β respectively) and measure the corresponding spring forces behind those points, we achieve complete input-observability on the detector. This statement is justified in the next sections. By measuring the forces behind those points, our model can be updated in terms of the measured quantities/outputs:

$$\begin{aligned} \mathbf{y} &= \begin{bmatrix} y_1 \\ y_2 \end{bmatrix} \\ &= \begin{bmatrix} kr(c_\psi s_\theta s_\alpha - s_\psi c_\alpha) \\ kr(c_\psi s_\theta s_\beta - s_\psi c_\beta) \end{bmatrix} \end{aligned} \tag{13}$$

2) Linearized Equations of Motion: In this section we linearize the equations of motion in order to simplify and study them further. For small values of $\mathbf{x} = [\theta\ \dot{\theta}\ \psi\ \dot{\psi}]^T$ (small motions of the drum) we can linearize Eq. [8, 9] and also Eq. [10, 11] and get:

$${}^{\mathcal{K}}M_{k,x}(\mathbf{x}) \approx kr^2(s_\kappa^2\theta - s_\kappa c_\kappa \psi) \tag{14}$$

$${}^{\mathcal{K}}M_{k,y}(\mathbf{x}) \approx kr^2(c_\kappa^2\psi - s_\kappa c_\kappa \theta) \tag{15}$$

$${}^{\mathcal{K}}M_{b,x}(\mathbf{x}) \approx br^2(s_\kappa^2\dot{\theta} - s_\kappa c_\kappa \dot{\psi}) \tag{16}$$

$${}^{\mathcal{K}}M_{b,y}(\mathbf{x}) \approx br^2(c_\kappa^2\dot{\psi} - s_\kappa c_\kappa \dot{\theta}) \tag{17}$$

In addition we can linearize the measurements from the force sensors (Eq. [13]) and get:

$$\mathbf{y} \approx \begin{bmatrix} kr(s_\alpha\theta - c_\alpha\psi) \\ kr(s_\beta\theta - c_\beta\psi) \end{bmatrix} \tag{18}$$

Combining Eq. [12] with Eq. [14-18] we can write the system of equations in matrix form, namely:

$$\dot{\mathbf{x}} = \mathbf{A}\mathbf{x} + \mathbf{B}\mathbf{d} \tag{19}$$

$$\mathbf{y} = \mathbf{C}\mathbf{x} \tag{20}$$

where the system matrices are given in Eq. [21-23]. Note here that disturbance vector from the occurrence of leaks at the circumference can be written as:

$$\mathbf{d} = \begin{bmatrix} d_1 \\ d_2 \end{bmatrix} = \begin{bmatrix} -F_z R s_\phi \\ F_z R c_\phi \end{bmatrix}$$

In the proposed and prototyped leak detector we placed $n = 4$ springs at points $\mathcal{K}_1, \mathcal{K}_2, \mathcal{K}_3$ and $\mathcal{K}_4$. Those points find themselves at equal distances $r = 17.5mm$ from the center of the gimbal G. More specifically, the enclosed angles were designed to be equal to (see Fig. 4):

$$\begin{cases} \kappa_1 = \pi/4 \\ \kappa_2 = 3\pi/4 \\ \kappa_3 = 5\pi/4 \\ \kappa_4 = 7\pi/4 \end{cases} \tag{24}$$

We need to mention here that with the specific selection of enclosed angles (Eq. [24]), the dynamics become further simplified and completely uncoupled for the θ, ψ motions. This is because elements $A_{2,3}, A_{2,4}$ and $A_{4,1}, A_{4,2}$ in Eq. [21] become identically equal to zero. The latter fact is very important, because, as the linear model now predicts, the drum is able to pivot about axes x and y independently. However, we know that there exists weak nonlinear coupling, that we neglected during linearization.

$$\mathbf{A} = \begin{bmatrix} 0 & 1 & 0 & 0 \\ \frac{-1}{I_{xx}} \sum_{i=1}^{4} kr^2 s_{\kappa_i}^2 & \frac{-1}{I_{xx}} \sum_{i=1}^{4} br^2 s_{\kappa_i}^2 & \frac{1}{I_{xx}} \sum_{i=1}^{4} kr^2 s_{\kappa_i} c_{\kappa_i} & \frac{1}{I_{xx}} \sum_{i=1}^{4} br^2 s_{\kappa_i} c_{\kappa_i} \\ 0 & 0 & 0 & 1 \\ \frac{1}{I_{yy}} \sum_{i=1}^{4} kr^2 s_{\kappa_i} c_{\kappa_i} & \frac{1}{I_{yy}} \sum_{i=1}^{4} br^2 s_{\kappa_i} c_{\kappa_i} & \frac{-1}{I_{yy}} \sum_{i=1}^{4} kr^2 c_{\kappa_i}^2 & \frac{-1}{I_{yy}} \sum_{i=1}^{4} br^2 c_{\kappa_i}^2 \end{bmatrix} \tag{21}$$

$$\mathbf{B} = \begin{bmatrix} 0 & 0 \\ \frac{1}{I_{xx}} & 0 \\ 0 & 0 \\ 0 & \frac{1}{I_{yy}} \end{bmatrix} \tag{22}$$

$$\mathbf{C} = \begin{bmatrix} krs_\alpha & 0 & -krc_\alpha & 0 \\ krs_\beta & 0 & -krc_\beta & 0 \end{bmatrix} \tag{23}$$

C. Controllability & Observability

The properties of the system described in Eq. [19-20, 21-23] are discussed here. We claimed earlier that with the specific measurements/outputs described by Eq. [18], the detector can achieve complete input-observability. However, we still need to justify our selection for the values of parameters α and β (we mentioned that in our design we picked $\alpha = \pi/4$ and $\beta = 3\pi/4$).

To do so, we start by calculating the corresponding observability matrix. The complete derivation is tedious but straightforward and skipped in this paper for simplicity. By deriving the observability matrix, we can see that the system is indeed completely observable under most of the cases for the angles α and β (observability matrix is full rank). However, there are some special cases that make the system unobservable. To retain full observability one needs to place a sensor at point $\mathcal{A}$ and then select another point $\mathcal{B}$ at an angle β such that ("Observability Rule"):

$$\beta \neq \alpha + m\pi \text{ for } m = -1, 0, -1$$

Now we introduce the check for system controllability. The configuration of the proposed detector, that is described by the linear governing equations presented in the previous section, makes the system fully controllable (controllability matrix is full rank for the corresponding linear system). Again the complete derivation of the controllability matrix is tedious and straightforward and skipped in this paper for simplicity.

Observability is a measure for how well internal states of a system can be inferred by knowledge of its measurements. Our detector being controllable means that the external disturbances can move the internal states of a system from any initial state to any other final state in a finite time interval. *Finally, by having a system that is both controllable and observable, the system becomes input-observable.* Input observability simply means that a change in inputs/disturbances in a dynamic system can reflect itself in the change of measurements (outputs).

D. Sensitivity

After studying the observability and the controllability of the system, we now know what rule to follow in order to build a detector that is input-observable. However, we still need to justify the selection of the parameters α and β in our design. To do that, we study the sensitivity of the sensor readings to changes in the disturbances. Our goal is to design a detector with input-observability and with maximum sensitivity. Starting from Eq. [18] we can get:

$$\boldsymbol{\delta y} = \begin{bmatrix} kr(s_\alpha \delta\theta - c_\alpha \delta\psi) \\ kr(s_\beta \delta\theta - c_\beta \delta\psi) \end{bmatrix} \tag{25}$$

An infinitesimal rotation about axis along the unit vector $\hat{\mathbf{e}}_\phi$, of magnitude $\delta\chi$ can be written in vector form as $\boldsymbol{\delta\chi} = \delta\chi\hat{\mathbf{e}}_\phi$. Equivalently we can write:

$$\boldsymbol{\delta\chi} = \underbrace{-\delta\chi s_\phi}_{\delta\theta}\,\hat{\mathbf{e}}_\mathbf{x} + \underbrace{\delta\chi c_\phi}_{\delta\psi}\,\hat{\mathbf{e}}_\mathbf{y} \tag{26}$$

Substituting back to Eq. [25] gives:

$$\boldsymbol{\delta y} = \begin{bmatrix} -k\delta\chi r(s_\alpha s_\phi + c_\alpha c_\phi) \\ -k\delta\chi r(s_\beta s_\phi + c_\beta c_\phi) \end{bmatrix} \tag{27}$$

Maximizing the above relations will maximize the sensitivity of the detector. By doing so we get for the optimal parameters ("Optimality Rule"):

$$\begin{cases} \alpha^\star = \phi + m\pi \text{ for } m = 0, 1 \\ \beta^\star = \phi + m\pi \text{ for } m = 0, 1 \end{cases}$$

To derive the previous result and come up with the optimal values for the parameters, we kept the spring stiffness k and the radial distance of the sensors r constant. However, one can easily infer that increasing either k or r will increase the sensitivity of the readings to inputs/disturbances.

The Optimality Rule implies that the maximum sensitivity is achieved when the sensors are placed either at the same angle as the leak, ϕ, or π away from it. Unfortunately, one cannot control where the leak will happen, since it can occur anywhere around the circumference of the pipe. Thus, placement of the sensors cannot be predetermined explicitly in order to increase sensitivity of the readings.

In this design we select $\alpha = \pi/4$ and $\beta = 3\pi/4$. By this selection we guarantee observability, since our design follows the Observability Rule . In addition, by placing the two sensors at orthogonal directions, we make sure that the maximum sensitivity directions of the two sensors on the drum do not overlap and are optimally spread out on the perimeter of the drum. More specifically, points $\mathcal{A}$, $\mathcal{B}$ now coincide with points $\mathcal{K}_1$, $\mathcal{K}_2$ (Fig. 4) on our proposed detector.

IV. Experimental Results and Validation

In this section the concepts we discussed in this paper are validated. Towards this goal a detector prototype was manufactured and system identification experiments were carried out in order to understand the dynamics under consideration. Moreover, signals for different incidence angles ϕ are demonstrated to illustrate the detector's input-observability.

A. Prototype Development & System Identification

A prototype of the proposed robotic detector was manufactured. To do this, most of the parts were built using a Fortus 250mc 3D printer from Stratasys and made out of ABS material. Additionally, the shaft (part [d] in Fig. 3) was manufactured from aluminum. The springs that we used were rated at $1.49N/mm$. Finally, for the force measurements we used two FSR 400 force sensors from Interlink Electronics under $8k\Omega hm$ voltage division. Those sensors are mounted on points $\mathcal{A}$ and $\mathcal{B}$ on the drum behind the linear springs.

Initially, we wanted to test whether the system behaves like a second order system for each of the two "uncoupled" degrees of freedom. If this is the case, we expect the transfer functions from disturbances to output forces to be of the form:

$$\begin{cases} \frac{Y_1(s)}{D_1(s)} = \frac{Y_1(s)}{-F_z(s)Rs_\phi} = \frac{K_1}{R}\frac{w_{n,1}^2}{s^2+2\zeta_1 w_{n,1}s+w_{n,1}^2} \\ \frac{Y_2(s)}{D_1(s)} = \frac{Y_2(s)}{-F_z(s)Rs_\phi} = \frac{K_1}{R}\frac{w_{n,1}^2}{s^2+2\zeta_1 w_{n,1}s+w_{n,1}^2} \\ \frac{Y_1(s)}{D_2(s)} = \frac{Y_1(s)}{F_z(s)Rc_\phi} = -\frac{K_2}{R}\frac{w_{n,2}^2}{s^2+2\zeta_2 w_{n,2}s+w_{n,2}^2} \\ \frac{Y_2(s)}{D_2(s)} = \frac{Y_2(s)}{F_z(s)Rc_\phi} = \frac{K_2}{R}\frac{w_{n,2}^2}{s^2+2\zeta_2 w_{n,2}s+w_{n,2}^2} \end{cases} \quad (28)$$

This can be proven by manipulating Eq. [19, 20] along with Eq. [21-23] and transforming them into standard transfer function form.

In order to evaluate the various parameters involved in the previous equations we performed system identification experiments. This was done by imposing impulsive in nature torques about axes x and y independently and try to fit second order models to the output signals. The results showed that the system indeed behaves like a second order system for each of the two degrees of freedom (see various responses in Fig. 5 that look second-order). Estimated parameters from the system identification experiments are summarized in Table I.

Name of Variable	Estimated Value via SysID
K_1	4.24
$w_{n,1}$	159.42 rad/sec
ζ_1	0.077
K_2	4.15
$w_{n,2}$	146.63 rad/sec
ζ_2	0.118

TABLE I
System ID values

B. Observability Demonstration

To illustrate input-observability of the proposed mechanism we demonstrate the reaction signals captured from the two force sensors. Impulsive in nature forces/torques were generated at different angles $\phi_i = \pi i/4$ for $i = 0, 1...7$ and results are shown in Fig. 5.

More specifically, we imposed impulsive inputs to the drum at different angles around the circumference and observed the captured output signals. We can see that each input disturbance (at ϕ_i) results in a distinct combination of output signals, as expected. The latter statement implies that the system is input-observable, as explained earlier in the paper. Indeed, as mentioned before, the system's response looks like second order for each degree of freedom as expected.

However, since we showed in this paper that the inputs/disturbances to our leak detector are observable, the question remaining is how to reconstruct the inputs. By doing so one may be able to recover information about the magnitude of leaks that is very useful for the operation of the robotic detection. Reconstruction of inputs/disturbances, has been investigated by researchers in the past [15] and is outside the scope of this paper.

V. Conclusions and Future Work

In this paper a detection system for in-pipe robotic inspection is proposed. Detection in based on the presence of a pressure gradient in the neighborhood of leaks. The latter phenomenon can then be translated into force measurements via a carefully designed and instrumented mechanism. Initially, an analytic dynamic model of the mechanism is derived and then simplified via linearization. In addition, the system is designed to be both controllable and observable and thus, input-observable. Finally, a prototype of the proposed detector is built to validate the concepts discussed in this paper and input-observability is demonstrated via experiments.

Our future works include the development of algorithms for input reconstruction. Input reconstruction would be very useful in practice, since the estimation of the input/disturbance force F_z would lead to the estimation of the size of the leak as implied by Eq. [2] and was discussed earlier in the paper. We are also working towards the development of algorithms for reliable leak identification and localization. Finally, we plan to perform further experiments and conduct testing of the detector in many pipe configurations under different working media (gas, water, oil). Last, but not least we plan to conduct experiments in real sections and real leaks.

Acknowledgments

The authors are very grateful to You Wu and Fred Moore for their support and help in this work.

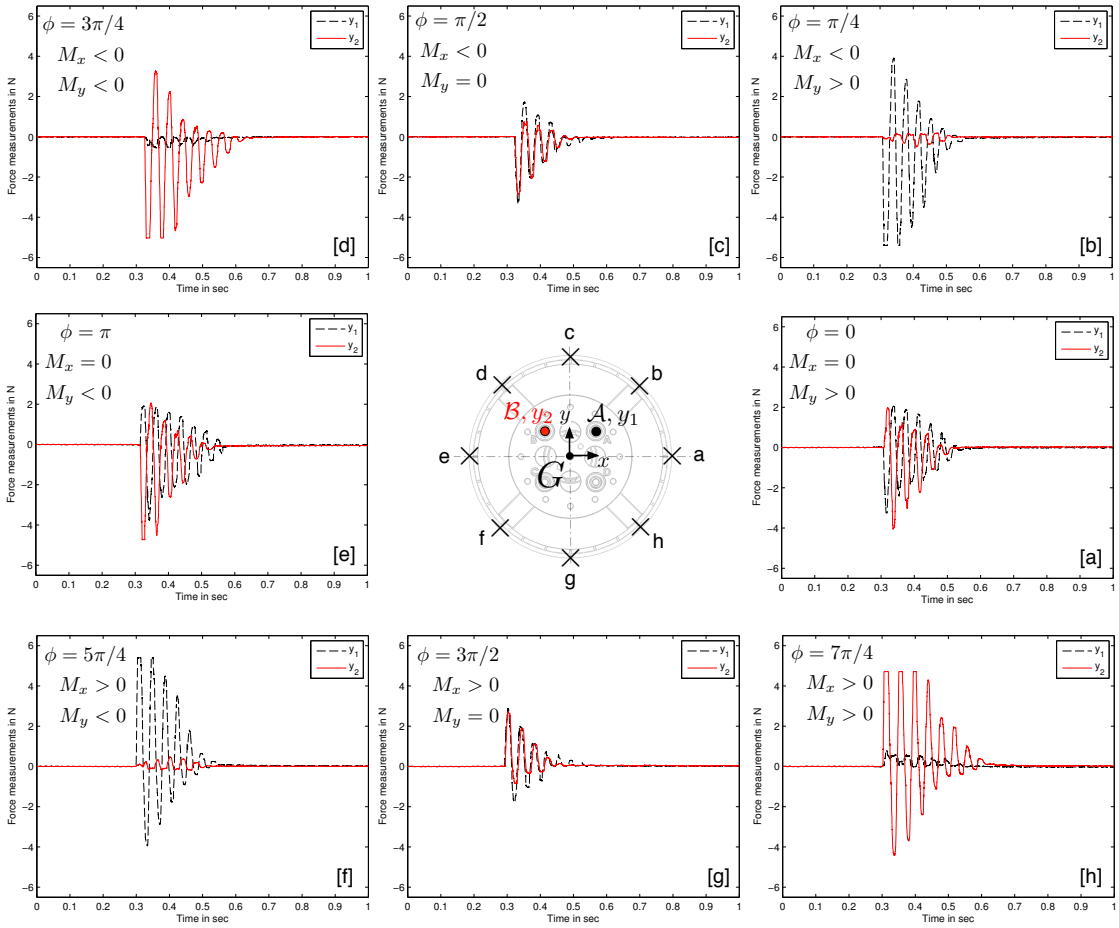

Fig. 5. Experimental demonstration of the input-observability of the proposed robotic detector. Impulsive forces at different angles on the drum are applied and output forces are measured with force sensors installed on points $\mathcal{A}$ and $\mathcal{B}$. For all figures [a] - [h] output from sensor at point $\mathcal{A}$, y_1 is depicted in black dashed line, while output from the second sensor at point $\mathcal{B}$, y_2 is depicted in red solid line. For each different input (at an angle ϕ_i) a distinct combination of output signals is observed, i.e. input-observability.

The authors would like to thank the King Fahd University of Petroleum and Minerals in Dhahran, Saudi Arabia, for funding the research reported in this paper through the Center for Clean Water and Clean Energy at MIT and KFUPM under Project Number R7-DMN-08.

The first author would like to thank the Onassis Public Benefit Foundation for the award of a prestigious scholarship throughout this work.

REFERENCES

[1] Vickers A. L. , "The future of water conservation: Challenges ahead," *Water Resources Update, Universities Council on Water Resources*, vol. 114, pp. 49–51, 1999.

[2] Senator Edward J. Markey, "America Pays for Gas Leaks. Natural Gas Pipeline Leaks Cost Consumers Billions." *Report*, 2013.

[3] Mays L., *Water Distribution Systems Handbook*. McGraw-Hill, 2000.

[4] Hunaidi O., Chu W., Wang A. and Guan W., "Leak detection method for plastic water distribution pipes," *Advancing the Science of Water, Fort Lauderdale Technology Transfer Conference, AWWA Research Foundation*, pp. 249–270, 1999.

[5] Fuchs H. V. and Riehle R., "Ten years of experience with leak detection by acoustic signal analysis," *Applied Acoustics*, vol. 33, pp. 1–19, 1991.

[6] Hunaidi O. and Chu W., "Acoustical characteristics of leak signals in plastic water distribution pipes," *Applied Acoustics*, vol. 58, pp. 235–254, 1999.

[7] Bracken M. and Hunaidi O., "Practical aspects of acoustical leak location on plastic and large diameter pipe," *Leakage 2005 Conference Proceedings*, no. 448-452, 2005.

[8] Kurtz D. W., "Developments in a free-swimming acoustic leak detection system for water transmission pipelines," *ASCE Conf. Proc.*, vol. 25, no. 211, 2006.

[9] Bond A., Mergelas B. and Jones C., "Pinpointing leaks in water transmission mains," *ASCE Conf. Proc.*, vol. 91, no. 146, 2004.

[10] Schempf H., Mutschler E., Goltsberg V., Skoptsov G., Gavaert A. and Vradis G., "Explorer: Untethered real-time gas main assessment robot system," *Proc. of Int. Workshop on Advances in Service Robotics (ASER)*, 2003.

[11] Choi H-R. and Roh S-G, "Differential-drive in-pipe robot for moving inside urban gas pipelines," *Transactions on Robotics*, vol. 21, no. 1, 2005.

[12] Chatzigeorgiou D., Wu Y., Youcef-Toumi K. and Ben Mansour R., "Reliable sensing of leaks in pipelines," *ASME Dynamic Systems and Controls Conference (DSCC)*, 2013.

[13] Chatzigeorgiou D., Ben-Mansour R., Khalifa A. and Youcef-Toumi K., "Design and evaluation of an in-pipe leak detection sensing technique based on force transduction," *ASME International Mechanical Engineering Congress & Exposition (IMECE2012)*, 2012.

[14] Ben-Mansour R, M.A. Habib, A. Khalifa, K. Youcef-Toumi and D. Chatzigeorgiou, "A computational fluid dynamic simulation of small leaks in water pipelines for direct leak pressure transduction," *Computer and Fluids*, p. doi:10.1016/j.compfluid.2011.12.016, 2012.

[15] M. Hou and R. Patton, "Input observability and input reconstruction," *Automatica*, vol. 34, no. 6, pp. 789 – 794, 1998.